Aerosol vertical distribution and sources estimation at a site of the Yangtze River Delta region of China

Wenzhi Fan, Kai Qin, Jian Xu, Limei Yuan, Ding Li, Zi Jin, Kefei Zhang

PII: S0169-8095(18)30764-6
DOI: https://doi.org/10.1016/j.atmosres.2018.11.002
Reference: ATMOS 4407

To appear in: *Atmospheric Research*

Received date: 13 June 2018
Revised date: 1 November 2018
Accepted date: 4 November 2018

Please cite this article as: Wenzhi Fan, Kai Qin, Jian Xu, Limei Yuan, Ding Li, Zi Jin, Kefei Zhang , Aerosol vertical distribution and sources estimation at a site of the Yangtze River Delta region of China. Atmos (2018), https://doi.org/10.1016/j.atmosres.2018.11.002

Aerosol vertical distribution and sources estimation at a site of the Yangtze River Delta region of China

Wenzhi Fan[a], Kai Qin[a,*] qinkai@cumt.edu.cn, Jian Xu[b], Limei Yuan[a], Ding Li[a], Zi Jin[c], Kefei Zhang[a]

[a]School of Environment Science and Spatial Informatics, China University of Mining and Technology, Xuzhou, China
[b]German Aerospace Center, Remote Sensing Technology Institute, Weßling, Germany
[c]Wuxi CAS Photonics Corporation, Wuxi, China

[*]Corresponding author.

Abstract

The vertical distribution characteristics of aerosols are key uncertain factors for studying the effect on radiative forcing and trans-regional transport of pollutants. This paper used three years (2013-2015) LiDAR measurements at a site in the Yangtze Delta region of China to investigate the aerosol vertical distribution and transport sources of aerosol-aloft by using the Potential Source Contribution Function (PSCF) and Concentration-Weighted Trajectory (CWT) models. The results indicated that there were 230 haze days accounted for 21% of all the days, including 142 damp haze days and 88 dry haze days during the study period. The aerosols below 2 km accounted for more than 89% of the total aerosol optical depth (AOD). Compared to other seasons, aerosols in winter were more likely to accumulate below 1 km (>69%). In summer, although atmospheric convention was strong leading to a high planetary boundary layer height (PBLH) and the concentration of $PM_{2.5}$ was low, the AOD was largest because of high relative humidity that caused hygroscopic growth of particles. Due to the stable weather condition in winter, the PBLH was low with the largest concentration of $PM_{2.5}$, so the occurrence of haze days was most frequent. The PSCF and CWT results revealed that the high-level aerosols mainly came from local areas; the CWT model showed considerable long-distance transports of dust from northern/northwestern China, as far as Mongolia, Gansu Province and Xinjiang Uygur Autonomous Region, in spring, autumn and winter. Southern sources were more obvious in winter that could contribute more anthropogenic aerosols and biomass burning emissions.

Keywords: Aerosol, LiDAR, Vertical distribution, Yangtze River Delta;

1. Introduction

China has experienced a rapid industrialization and urbanization over the last decades, resulting in a heavy aerosol loading (Che et al., 2014; Guo et al., 2016a; Shang et al., 2017; Qin et al., 2018a). Particularly, frequent haze episodes with record-breaking $PM_{2.5}$ (particulate matter with diameters smaller than 2.5 μm in aero-dynamics) level have been observed over densely populated urban regions, e.g. the Yangtze River Delta (YRD). The YRD is the alluvial plain in front of the sea the Yangtze River enters, including Shanghai, Jiangsu Province and Zhejiang Province (Fig.1). It is one of the largest industrial and agriculture productive areas, suffering from severe air pollution due to the anthropogenic emissions (Cheng et al., 2015; He et al., 2010; Kang et al., 2016; Wang et al., 2015).

Given that aerosol properties vary significantly as a function of height (Cho et al., 2017; Cohen et al., 2018; Guo et al., 2016b), measurements of aerosol vertical distribution are critical for assessing the effects of aerosols on radiative forcing and an important piece of information to improve satellite-based ground $PM_{2.5}$ concentration estimation (Han et al., 2015). LiDAR (Light Detection And Ranging) had been widely used as a significant means to detect the vertical distribution and spatio-temporal evolution of aerosols (Baars et al., 2016). He et al. (2008) used micro pulse LiDAR (MPL) measurements acquired from May 2003 to June 2004 to illustrate seasonal variations of aerosol optical depth (AOD) and Planetary Boundary Layer Height (PBLH) in Hong Kong, finding about 64% of the monthly mean AOD was contributed by aerosols within the planetary boundary layer. Liu et al. (2012) analyzed the seasonal variations of aerosol vertical distribution at a site in the YRD region of China based on the MPL data during 2008-2009. They reported some aerosol-aloft were traced back to northern/northwestern China, as far as Mongolia and Siberia, in spring, autumn and winter, but the authors used fixed heights of 0.5 km and 2.5 km as the arrival heights. Chew et al. (2016) found that the vertical distribution of aerosols had an important impact for the relationship between AOD and ground particulate matter in Singapore and the modified aerosol scale heights were used to improve the estimation of the hourly surface $PM_{2.5}$ concentrations. Qin et al. (2016) revealed a trans-boundary haze transport in China using ground-based LiDAR and CALIPSO satellite data. Wong et al. (2017) suggested that aerosol vertical profiles offered by LiDAR measurements were very helpful in understanding aerosol pollution variability and trends.

Transported aerosol layers within the residual boundary layer may be mixed into the surface by way of the entrainment zone (Atwood et al., 2013; Cottle et al., 2014; Wu et al., 2012) and increased the surface aerosol loading when aerosol concentration in the residual layer was higher. Therefore it is necessary to explore the sources of the aerosol-aloft. Based on the backward trajectories, statistics methods had been used to gain insights into the source locations and prevailing transport pathways of airborne particles and gases (Aab et al., 2014; Guo et al., 2017). The potential source contribution function (PSCF) is simple method that links residence time in upwind areas with high concentrations through a conditional probability field (Ashbaugh et al., 1985) . Wong et al. (2013) combined Aerosol Robotic Network (AERONET) data, backward trajectories, and the PSCF model to identify probable transport pathways and magnitudes of aerosols over Hong Kong, the results showed aerosols were mainly from local, including Hong Kong itself and the neighbouring region. Because the PSCF method cannot perform quantitative analysis of the pollutants, Stohl (1996) refined this method by redistributing the concentration fields (e.g. $PM_{2.5}$), and Hsu et al. (2003) further refined it to a concentration-weighted trajectory (CWT) method. Wang et al. (2006a) used PM_{10} data combined with PSCF and CWT models to evaluate the dust transport pathways and sources of Xian in spring 2001 to 2003. This study showed the advantages that were gained by using multiple trajectory statistic methods and in recognizing the limitations of each.

However, most of the studies mentioned above focused on vertical distribution of case studies in short-term haze events. Besides, previous studies had paid little attention to long-term high-level aerosols in each season, and generally used an empirical height value as start locations. The objective of this study was to reveal long-term vertical distribution of aerosols and analyze their influencing factors during haze and haze-free periods over the YRD region from 3-years LiDAR observations, which were helpful for understanding the formation of haze and provided vertical profiles for estimating ground $PM_{2.5}$. Moreover, source analysis of aerosol-aloft were evaluated by combining LiDAR observations with PSCF and CWT models.

2. Data and methods

2.1. Site and Measurements

The LiDAR site used in the study is in downtown Wuxi, which is in southern Jiangsu province, a part of the YRD region and covers a coastline of the Yangtze River in the north and two separate coasts of Lake Tai. A high-energy LiDAR system (model: AGHJ-I-LiDAR, right in Fig. 1), manufactured by Wuxi CAS Photonics Corporation, was operated on the roof of the 11th floor, Block C of China Sensor Network Innovation Park, Wuxi City, Jiangsu Province (31.5°N, 120.37°E), since 2011. The LiDAR emits green light at 532 nm with energy about 20 mJ and a pulse repetition rate of 20 Hz. Its time resolution is 5-minute and the vertical resolution is 7.5 m. The blind zone height of incomplete after pulse correction (overlap area) is approximately 0.3 km and it should be noted that in this paper, the full overlap height is about 500m (Fig.2). The raw measurements with a high-temporal resolution were averaged in 1-hour intervals to improve the signal-to-noise ratio. Here, hourly averaged LiDAR measurements from January 2013 to December 2015 were used. According to the extinction coefficient greater than 2 km^{-1}, and the magnitude of the depolarization ratio, the cloud and rain periods were identified (Li et al., 2011; 2013; 2015; Zhao et al., 2014; Zhang et al., 2018), after removing data with cloud and rain time, a total of 11112 hourly profiles remained.

The signals received by LiDAR are energy values, and the optical property values are usually obtained by solving the LiDAR equation. The corresponding LiDAR factors should be amended before the processing of the LiDAR data. The modified LiDAR equation is as follows:

$$P(r) = CE\frac{1}{r^2}\beta(r)\,exp\left[-2\int_0^r \sigma(z)dz\right] \qquad (1)$$

where P is the atmospheric backscattering echo power (W) at the height r (km) received by LiDAR, E is the LiDAR launching energy (μJ), C is the LiDAR system constant (W·km^3·sr), $\beta(r)$ and $\sigma(r)$ are the total atmospheric backscattering coefficient and the extinction coefficient (km^{-1}·sr, and km^{-1}) at height r (km), respectively. Since both are unknown factors, they need to be retrieved using specific methods, which usually include the Collis Method (Collis and Russell, 1976), the Klett Method (Klett, 1981) and the Fernald Method (Fernald, 1984). Among these, the Fernald Method considering the atmosphere to be comprised of aerosols and air molecules is used widely. Thus, the Eq.(1) for this method can be written as follows:

$$P(r) = CE\frac{1}{r^2}[\beta_a(r) + \beta_m(r)]exp\left[-2\int_0^r [\sigma_a(z) + \sigma_m(z)]dz\right] \qquad (2)$$

where the subscripts a and m represent aerosols and air molecules, respectively. Because the two parameters $\beta_a(r)$ and $\sigma_a(r)$ are unknown and the other two parameters $\beta_m(r)$ and $\sigma_m(r)$ can be obtained using the U.S. standard atmospheric model, the extinction-to-backscattering ratio $S(r)$ is introduced in this method. The aerosol extinction-to-backscattering ratio and the air molecule extinction-to-backscattering ratio are defined as $S_a(r) = \sigma_a(r)/\beta_a(r)$ and $S_m(r) = \sigma_m(r)/\beta_m(r)$, respectively. Thus the optical properties of aerosols and air molecules can be obtained by solving Eq.(2).

The Fernald distant solving method was used in this paper. The height r_m(km) above the atmosphere where there is almost no aerosols is used to transform Eq.(2) as follows:

$$\sigma_a(r) = -\frac{S_a}{S_m}\sigma_m(r) + \frac{ln[P(r)]exp\left[2\left(\frac{S_a}{S_m}-1\right)\int_r^{r_m}\sigma_m(z)dz\right]}{\frac{lnP(r_m)}{\sigma_a(r_m)+\frac{S_a}{S_m}\sigma_m(r_m)} + 2\int_r^{r_m} ln[P(r)]exp\left[2\left(\frac{S_a}{S_m}-1\right)\int_r^{r_m}\sigma_m(\acute{z})d\acute{z}\right]dz} \qquad (3)$$

where S_a is the aerosol extinction-to-backscatter ratio between 20 and 70. Here we applied a value of 50 assuming urban and mineral mixtures at 532 nm (Mao et al., 2012), which could led to 20-30% uncertainties in data retrieval. S_m is the air molecule extinction-to-backscattering ratio of 8π/3 that can be provided by the U.S. standard atmosphere model, and r_m is the boundary height.

The AOD integrated from ground level to a certain altitude r (km) then can be calculated as follows:

$$\text{AOD} = \int_{r1}^{r2} \sigma_m(r)dr \qquad (4)$$

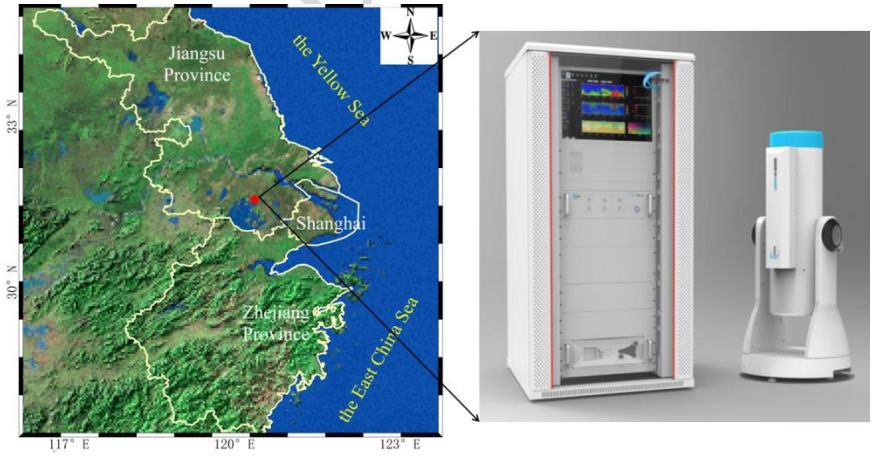

Fig.1. Elevation map of the Yangtze River Delta region plotted using ArcGIS software based on the Shuttle Radar Topography Mission 90 m digital elevation data. The red point is the location of Wuxi and the right figure is the LiDAR system.

2.2. Auxiliary Data

The $PM_{2.5}$, PM_{10} and meteorological data were obtained from Qingyue Open Environment Data Center (http://data.epmap.org/) to determine the haze days. This website collected $PM_{2.5}$ and PM_{10} data from the Chinese Ministry of Environmental Protection's National Real-Time Air Quality Reporting and meteorological data from China National Meteorological Information

Center. Although specific in-situ instruments are unknown, all the data has been processed using quality control standard. Combining with the two sets criteria for the definition of hazes issued by Chinese Ministry of Environmental Protection (Qin et al., 2018b) and China Meteorological Administration, we defined a haze day when the average concentration of $PM_{2.5}$ is above 75 μg/m^3, hourly mean ratio of $PM_{2.5}$ and PM_{10} concentrations is greater or equal to 60% and the visibility is less than 5 km for more than six consecutive hours. Furthermore, the haze days was classified as dry haze days when the relative humidity is less than 80% and as damp haze days when the relative humidity is between 80% and 95%.

2.3. Trajectory data and PSCF, CWT models

Five-day backward trajectories arriving at Wuxi in different seasons were calculated for every hour using the National Oceanic and Atmospheric Administration (NOAA) Hybrid Single Particle Lagrangian Integrated Trajectory Model (HYSPLIT4) trajectory model (Draxler and Hess, 1998). The National Centers for Environmental Prediction, Final Analyses (NCEP/FNL) archive data Global Data Assimilation System (GDAS) were used as meteorological data input to the model. In this paper, in order to determine the source of high-level aerosols, according to the vertical distribution of extinction coefficient based on the LiDAR data, we first screened out the periods under the influence of high-level aerosols during the haze period, and got the roughly average height of the aerosol-aloft layers in each season, which was 1400 m, 2400 m, 1300 m and 1500 m in spring, summer, autumn and winter, respectively. The above heights as the start locations input in HYSPLIT4 model were calculated for each trajectory.

Based on the above-generated backward trajectories, the Potential Source Contribution Function (PSCF) model and the Concentration-Weighted Trajectory (CWT) method were established by using TrajStat software (Wang et al., 2009). In this study, AOD values larger than 0.2 (Wong et al., 2013) in 1.0-3.5 km were used as the threshold criterion for application of the PSCF and the CWT models and the study area extended from 70°E to 140°E and from 15°N to 55°N including the entire Chinese mainland, the spatial resolution was 0.5×0.5° with 11200 grid cells in latitude and longitude. The PSCF model simulates the potential probability of source areas from designated receptors. The PSCF values for the grid cells in the study domain are calculated by counting the backward trajectory segment endpoints that terminate within each cell, which is expressed as (Han et al., 2007):

$$PSCF(ij) = (m_{ij}/n_{ij})W_{ij} \quad (5)$$

The number of endpoints that fall in the ijth cell is designated n_{ij} and the number of endpoints for the same cell having arrival times at the sampling site corresponding to AOD values higher than an arbitrarily set criterion is defined as m_{ij}. W_{ij} is an empirical weight function proposed by Zeng and Hopke (1989) to reduce the undue influence of small n_{ij} on the PSCF values:

$$W_{ij} = \begin{cases} 1.00 & n_{ij} > 3 \cdot Avg \\ 0.70 & Avg < n_{ij} \leq 3 \cdot Avg \\ 0.42 & 0.5 \cdot Avg < n_{ij} \leq Avg \\ 0.17 & 0 < n_{ij} \leq .5 \cdot Avg \end{cases} \quad (6)$$

where Avg is the average number of trajectory segment endpoints in all cells.

A limitation of the PSCF method is that grid can have the same PSCF value when sample concentration are either only slightly higher or much higher than the criterion. As a result, it can be difficult to distinguish moderate sources from strong ones, so it is necessary to introduce other method (Cheng et al., 2015; Zachary et al., 2018). In the Concentration-Weighted Trajectory (CWT) method, each grid cell is assigned a weighted concentration by averaging the sample concentration that has associated trajectories that crossed the grid cell as follows (Seibert et al., 1994).

$$C_{ij} = \frac{1}{\sum_{l=1}^{M} \tau_{ijl}} \sum_{l=1}^{M} C_l \, \tau_{ijl} \quad (7)$$

where C_{ij} is the average weighted concentration in the *ij*th cell, *l* is the index of the trajectory, *M* is the total number of trajectories, C_l is the concentration observed on arrival of trajectory *l*, and τ_{ijl} is the time spent in the *ij*th cell by trajectory *l*. A high value for C_{ij} implies that air parcel traveling over the *ij*th cell would be, on average, associated with high concentrations at the receptor. The arbitrary weighting function described above was also used in the CWT analysis to reduce the effect of the small values of C_{ij}. In this study, the trajectory residence time in the grid cells have been weighted by the observed AOD (C_l) corresponding to the arrival of each trajectory, so that the AOD values of each cell can be simulated.

3. Results and discussions

3.1 Variations of haze days

Based on the above definition, we counted the number of haze days over Wuxi during the 3-years from 2013 to 2015. According to the relative humidity, the haze days were furthermore divided into damp haze days and dry haze days. As shown in Table 1, there were 230 haze days, which mostly occurred in winter (108 days, December, January and February), followed by spring (56 days, March, April, May), autumn (40 days, September, October, November) and summer (26 days, June, July, August).

There were 142 damp haze days and 88 dry haze days. Winter had the most number of damp haze days (55 days), accounted for 50.9% of the corresponding haze days. And summer had least number of damp haze days (19 days) with 73.1% of the corresponding haze days, followed by spring (42 days, 75%) and autumn (26 days, 65%).

Table 1. Seasonal occurrence of haze days, damp and dry haze days in Wuxi from January 2013 to December 2015.

Season	Haze days	Damp haze days	Dry haze days

Spring	56	42	14
Summer	26	19	7
Autumn	40	26	14
Winter	108	55	53

3.2 Variations of aerosol extinction coefficient and AOD

As a basic parameter of aerosol optical property, extinction coefficient can reflect aerosol burden, and generally used to assess the aerosol vertical distribution. Previous studies (e.g., Zheng and Zhao, 2017) reported that the vertical structure of aerosol distribution exhibits a remarkable change with seasons. When we did not distinguish between haze and haze-free days (Fig.2), the total of 11112 hourly average aerosol extinction profiles were analyzed to derive the seasonal mean vertical profiles during 2013-2015. Of these profiles, 2976 were in spring, 2911 in summer, 3057 in autumn and 2168 in winter. Fig. 2 showed seasonal (blue lines), annual (red lines) mean, the median (black lines), the 5% and 95% percentile (green lines) profiles of aerosols extinction coefficient profiles at 532 nm. Horizontal lines represented standard deviations of the seasonal mean. The highest extinction coefficient occurred below 2.0 km, gradually decreased with altitude. The maximum value for annual mean extinction coefficient was about 0.4 km^{-1} at 0.5 km near the surface.

Spring and annual mean profiles of 2.0-3.5 km were coincident, while the annual mean was larger than spring below 2.0 km. The maximum mean value in spring was about 0.35 km^{-1}. The profiles of summer and autumn were analogous, 1.0-2.5 km values of summer and 0.5-2.0 km values of autumn were slightly larger than the annual mean values and other height profiles were overlapping. In winter, in addition to overlapping parts in 2.5-3.5 km, 1.0-2.5 km values were less than the annual mean values, which was converse below 1km, and the largest value of extinction coefficient was about 0.5 km^{-1}.

When we distinguished between haze and haze-free days (Fig.3), there was no doubt that the extinction coefficient of the haze periods was much larger than that of the haze-free periods. The maximum value of the extinction coefficient for all seasons at 0.5 km during haze-free periods was about 0.3-0.4 km^{-1}. The largest value appeared in winter, followed by autumn and summer, and with the smallest value occurred in spring. During the haze period, the largest extinction coefficient appeared in summer, reached 0.8 km^{-1} at 0.5 km, followed by winter (0.7 km^{-1}). And values of autumn and spring were similar, were about 0.6 km^{-1}.

Above 2.0 km, the profiles of haze and haze-free were overlapping in spring. As shown in Fig.3, the extinction coefficient during the haze periods was obviously greater than haze-free periods in 2.0-3.0 km in summer, which was magnified and displayed. If the data that had high-level aerosols were removed from profiles then new mean profiles (green line) were obtained, the green and blue lines were roughly coincident and the effects of aerosol-aloft will be discussed in detail in Section 3.4. Due to the higher PBLH during haze-free period in autumn, the extinction coefficient of haze-free period was larger than that of haze period in 1.5-2.0 km. In winter,

because of the stable weather condition, aerosols gathered below 2.0 km, and the profiles above 1.5 km were almost coincident.

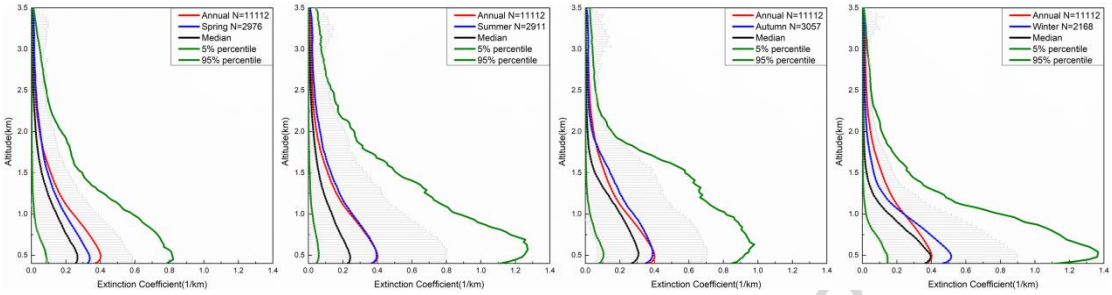

Fig.2. Seasonal (blue lines), annual (red lines) mean, the median (black lines) , the 5% and 95% percentile (green lines) profiles of aerosol extinction coefficient profiles at 532nm over Wuxi from January 2013 to December 2015. Horizontal lines represented standard deviations.

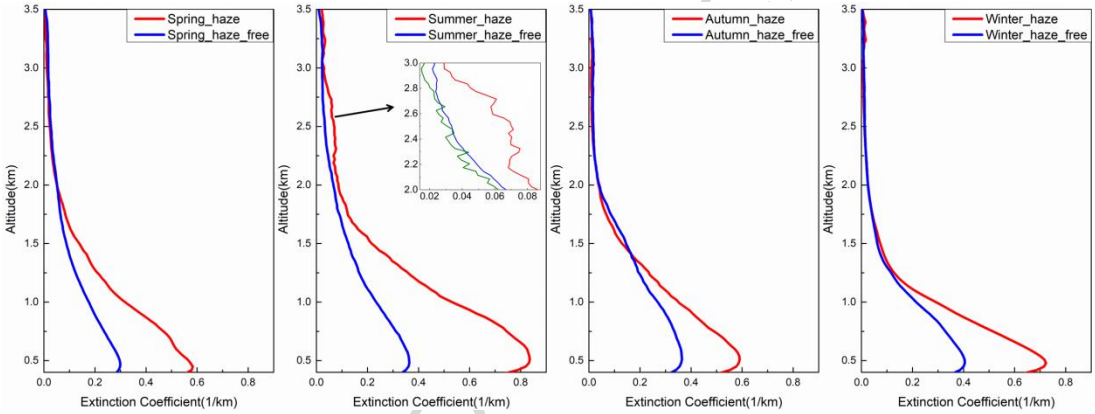

Fig.3. Seasonal mean profiles of aerosols extinction coefficient at 532nm on haze days (red lines) and haze-free days (blue lines) over Wuxi from January 2013 to December 2015. A magnification of the profile from 2.0 to 3.0 km was shown for summer.

The AOD is the integration of the atmospheric extinction coefficient in the vertical direction, reflecting the attenuation of the sunlight induced by aerosols, and is seen as an important indicator for evaluating aerosol concentration and atmospheric pollution. In this paper, the extinction coefficient obtained data from the LiDAR was used to calculate the AOD in different heights according to Eq.(4).

Tables 2 and 3 showed the ratios of AOD at different heights in Wuxi during haze and haze-free periods from January 2013 to December 2015. AOD1 meant AOD in 0.5-1.0 km, AOD2 meant AOD in 0.5-2.0 km and AOD3.5 meant AOD in 0.5-3.5 km. During the period of haze, the ratio of AOD2 to AOD3.5 exceeded 89% in all seasons, indicating that the most of aerosol were concentrated below 2.0 km during the haze days. The highest ratio appeared in winter (95.0%) and the lowest in summer (89.1%). In winter, about 69.3% aerosol was confined to below 1.0 km, followed by 58.2%, 55.9%, 53.1% in autumn, spring and winter, respectively. Compared to other seasons, aerosols in winter were more likely to accumulate below 1 km. Similar to seasonal distribution of AOD during the haze period, the ratios of AOD2 to AOD3.5 of haze-free days were over 85% for all seasons. The largest proportion occurred in winter (92.8%), followed by autumn

(91.9%), summer (86.0%) and spring (85.5%). Moreover the ratios of AOD1 to AOD3.5 were 61.7%, 49.1%, 47.2% and 46.5% in winter, autumn, spring and summer, respectively.

Table 2. The ratios of AOD at different heights during haze period in Wuxi from January 2013 to December 2015.

Season	AOD1/AOD3.5	AOD2/AOD3.5
Spring	55.9%	92.7%
Summer	53.1%	89.1%
Autumn	58.2%	94.7%
Winter	69.3%	95.0%

Table 3. The ratios of AOD at different heights during haze-free period in Wuxi from January 2013 to December 2015.

Season	AOD1/AOD3.5	AOD2/AOD3.5
Spring	47.2%	85.5%
Summer	46.5%	86.0%
Autumn	49.1%	91.9%
Winter	61.7%	92.8%

3.3. Influence factors to aerosol vertical distribution

There were many factors affecting the vertical distribution of aerosols. The following were mainly described in terms of fine particles, relative humidity and planetary boundary layer height.

3.3.1 $PM_{2.5}$ and PM_{10}

Table 4 showed seasonal average concentrations of $PM_{2.5}$, PM_{10} and their ratios in Wuxi during haze period from January 2013 to December 2015. The ratios of $PM_{2.5}$ to PM_{10} in all seasons exceeded 69%, indicating that $PM_{2.5}$ was the main pollutant in Wuxi. The average concentration of $PM_{2.5}$ in winter was the highest, reached 143 μg/m^3, and the highest proportion appeared simultaneously, which meant that the impact of PM_{10} was weaker compared with other seasons. Seasonal average concentrations of $PM_{2.5}$ were 100 μg/m^3, 90 μg/m^3 and 84μg/m^3 in autumn, spring and summer, respectively. $PM_{2.5}$ accounted for 69.8% and 69.4% of PM_{10} in spring and autumn, respectively, and they were more susceptible to PM_{10}.

Table 4. Seasonal averages concentrations of $PM_{2.5}$, PM_{10} and their ratios in Wuxi during haze period from January 2013 to December 2015.

Season	$PM_{2.5}$（μg/m^3）	PM_{10}（μg/m^3）	$PM_{2.5}$/ PM_{10}
Spring	90	129	69.8%
Summer	84	115	73.0%
Autumn	100	144	69.4%
Winter	143	182	78.6%

3.3.2 Relative humidity

When the relative humility is higher than 60%, the relative humidity itself or the water absorbed by aerosol becomes a dominant controlling factor. For pollution or urban aerosol, when

the relative humidity is 70-80%, water contributes 50% or more of the total quantity of aerosols (Liu et al., 2016). Therefore as the relative humidity increases, the scattering ability of the aerosol is enhanced. Condensed water typically contributes 40% to the light scattering budget in the Yangtze River Delta region of China (Xu et al., 2002). As shown in Table 5, the relative humidity was 78%, 74%, 74% and 71% in summer, spring, autumn and winter. According to the Fig. 3 and the Table 4, although the concentration of $PM_{2.5}$ in summer was the lowest, the extinction coefficient in 0.5 km was the highest, which was due to the effect of the hygroscopic aerosols. The relative humidity in winter was the lowest, but $PM_{2.5}$ in winter was much higher than that of other seasons, so the extinction coefficient also can reach 0.7 km^{-1} in 0.5 km.

During haze-free days, the maximum relative humidity in summer was 74%, followed by autumn (69%), winter (66%) and spring (65%). Relative humidity of haze period was larger than that of haze-free period, which suggested that relative humidity might promote the formation of haze.

Table 5. Seasonal averages relative humidity in Wuxi during haze and haze-free periods from January 2013 to December 2015.

	haze days	haze-free days
Spring	74	65
Summer	78	74
Autumn	74	69
Winter	71	66

3.3.3 Planetary boundary layer height

In general, the planetary boundary layer height (PBLH) retrieved in the LiDAR signals is the rapid attenuation of the echo signals (Hennemuth and Lammert, 2006; Liu et al., 2018; Mao et al., 2013).The PBLH can be obtained by the visual and qualitative interpretation based on the vertical distribution of aerosol extinction coefficient mapping from the LiDAR. Fig. 4 showed hourly variations of the mean vertical distribution of aerosol particle extinction coefficient at 532 nm in Wuxi in different seasons of haze and haze-free periods from January 2013 to December 2015. Therefore, the PBLH was the junction of light blue and dark blue backgrounds in Fig. 4. The PBLH varying from a few hundred meters to a few thousand meters is mainly composed of three parts: the mixing layer, the residual layer and the stable boundary layer. When the PBLH is low, the pollution on the surface cannot diffuse efficiently and congregates together, which is conducive to the formation of haze.

The diurnal variations of the PBLH in different seasons were roughly consistent. For every season, the lowest PBLH appeared at local 6:00 to 8:00 and reached peak point at 14:00 to 16:00. The daily change of the PBLH was closely related to solar radiation. From 8:00, the sun rose and the atmospheric turbulence was strengthened, so the PBLH started rising and reached the top in the afternoon. After that, as the solar radiation weakened, the atmospheric turbulence decreased and the PBLH began to decrease.

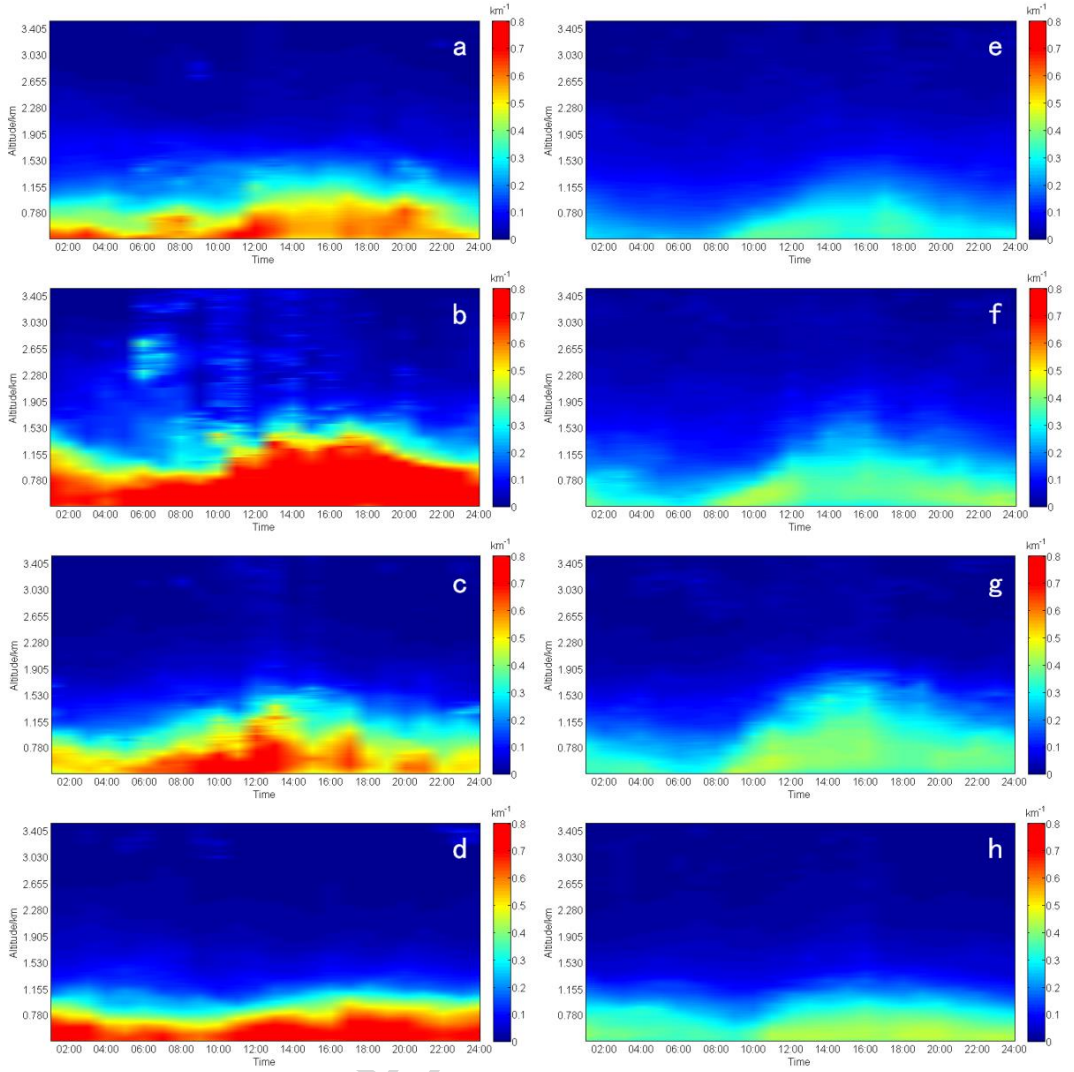

Fig.4. Hourly variations of vertical distribution of aerosols extinction coefficient at 532nm in Wuxi in spring (a), summer (b), autumn(c) and winter (d) of haze days and spring (e), summer (f), autumn(g) and winter (h) of haze-free days from January 2013 to December 2015.

In summer, the PBLH was the highest, reached 1.530 km around 14:00, which was related to the high temperatures and strong atmospheric turbulence activities. Because of the negative correlation between PBLH and particle concentration (Qu et al., 2017), the concentration of $PM_{2.5}$ in summer was the lowest, which was partly result of the high PBLH. The lowest PBLH was about 1 km in winter, which was due to the low temperature, stable weather conditions, thus the most of the aerosols gathered in the boundary layer and led to the largest concentration of $PM_{2.5}$. The PBLH was about 1.5 km and 1.2 km in autumn and spring, respectively that correlated with the relatively lower temperatures and strengthened winds.

During the haze-free period, the autumn PBHL reached a maximum at 14:00 and approached about 1.9 km that could be attributed to less rain and convective instabilities. This explained that the extinction coefficient of haze-free days was greater than that of haze days in 1.5-2.0 km in Fig. 3. The PBLH was about 1.5 km, 1.2 km and 1 km in summer, spring and winter, respectively.

3.4. Source analysis of aerosol-aloft based on PSCF and CWT models

As shown in Fig.5, the PSCF values indicate the probabilities of the potential source areas to high AOD loadings in Wuxi. The most extensive sources of long-distance aerosol-aloft transport were found in winter, while the local sources were dominant in summer due to the least number of haze days and overall low aerosol levels. In winter, there were two main sources from northwest and southwest regions. The northwest transport source to Wuxi was located in a place called "Northern High Dust Desert" (Zhang et al., 1998), and the Badain Juran desert was in its center in Inner Mongolia, then the dust were transported through Shaanxi, Shanxi, Henan and Anhui Provinces. The southwest sources came from eastern Hubei and Hunan Provinces. In spring, besides local sources, the regions such as northern Jiangsu and Zhejiang, northeastern Anhui, southwestern Shandong and southern Hebei, were important sources. In autumn, the distribution of PSCF map was not dispersed like spring and winter but gathered in the surrounding provinces.

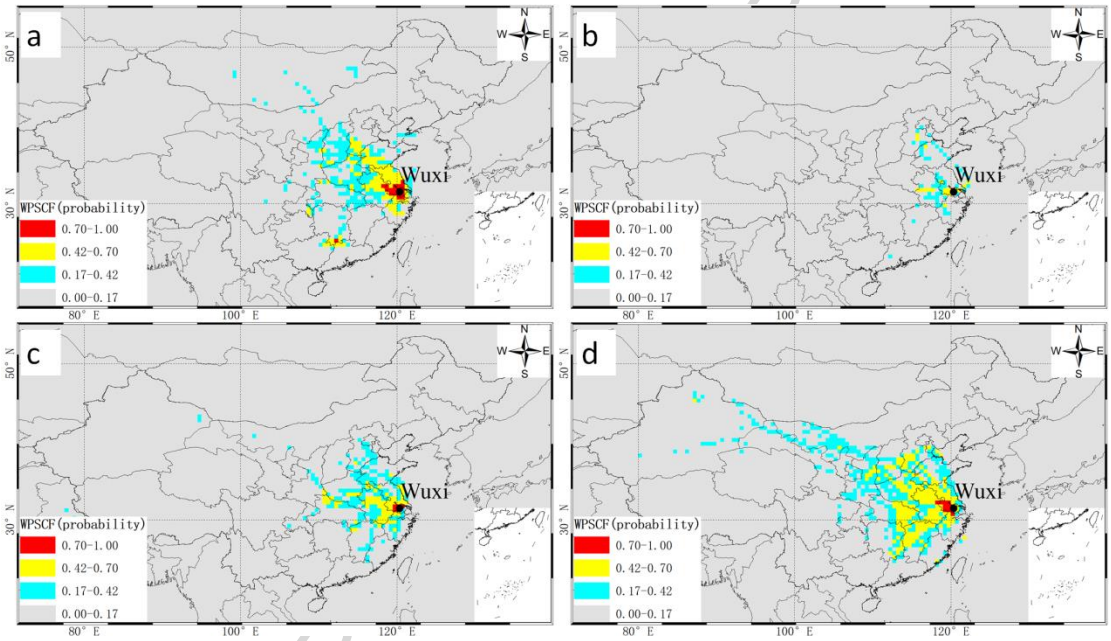

Fig.5. Potential source contribution function maps of 1.0-3.5km AOD in Wuxi in spring (a), summer (b), autumn (c) and winter (d) from January 2013 to December 2015.

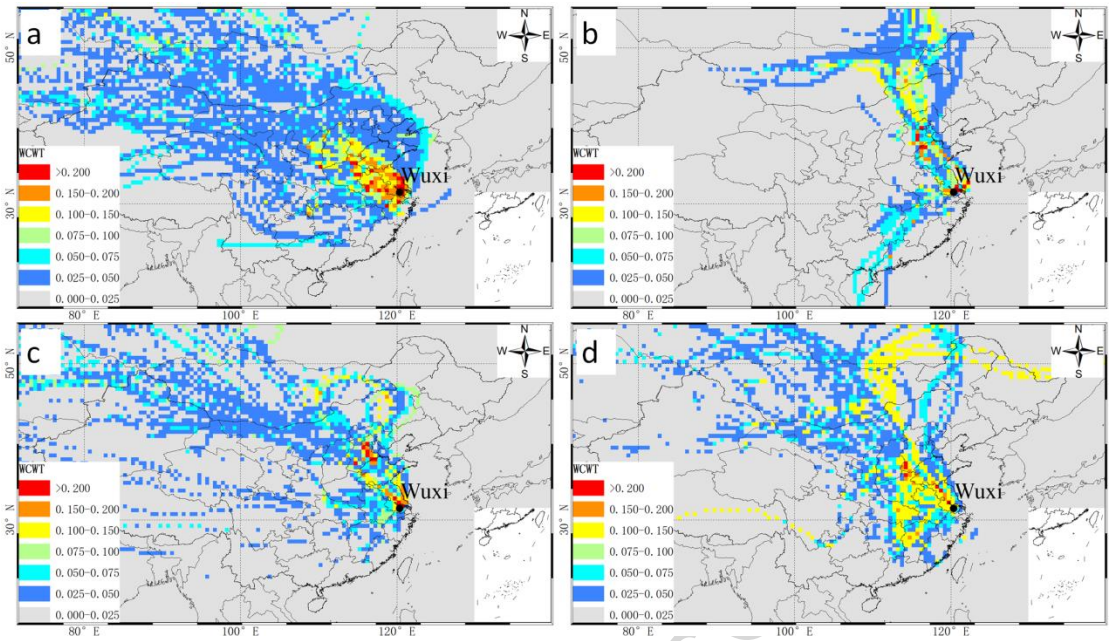

Fig.6. Concentration-weighted trajectory maps of 1.0-3.5km AOD in Wuxi in spring (a), summer (b), autumn (c) and winter (d) from January 2013 to December 2015.

As shown in Fig.6, the CWT analysis simulates the contribution from potential source zone to high AOD loadings in Wuxi. Generally, high weight values (>0.200) were located in the vicinity of Wuxi and thus quantifies the contribution from potential source regions. In spring, autumn and winter, aerosols from northern regions of China were widely distributed but their weight values were smaller around 0.025-0.050. Similar to the results of PSCF, the CWT model showed obvious contributions from southwardly sources. In addition, the CWT revealed that the contributions from northeast of Mongolian Plateau were considerable in summer and winter, which cannot be seen from the PSCF map.

Benefiting from LiDAR-derived aerosol-aloft information, our combined analysis using both PSCF and CWT models make it possible to comprehensively characterize the sources of aerosol transport to Wuxi. Long-distance transports of dust in Gansu, Inner Mongolia, and Xinjiang provinces with most concentrated desert distribution were important aerosol sources in Wuxi (Wang et al., 2006b; Yong et al., 2015), especially in spring. Unlike northern sources, due to their comparatively high precipitation and more vegetative cover, southern sources contributed more emissions of anthropogenic activities, such as biomass burning (Sun et al., 2018; Wu et al., 2017) and urban-industrial type aerosols (Kang et al., 2016).

4. Conclusion

Aerosol vertical distributions at a site of the Yangtze Delta region of China were investigated using three-years LiDAR measurements from January 2013 to December 2015. Furthermore, transport sources of aerosol-aloft were estimated using the Potential Source Contribution Function (PSCF) and Concentration-Weighted Trajectory (CWT) models. The major findings of this work are summarized as follows:

1. During the study period, there were 230 haze days, accounted for 21% of all the days, with the highest proportions in winter and the lowest proportions in summer.
2. Aerosol extinction coefficient profiles and AOD at different heights during haze periods revealed that most aerosols (> 89%) were concentrated below 2.0 km, aerosols in winter were more likely to accumulate below 1 km (>69%).
3. The lowest planetary boundary layer heights (PBLH) was found in winter, which aggravated accumulation of aerosols near surface resulting in the most frequent haze pollution. Although the PBLH in summer was highest, which was good for diffusion of aerosols, but the AOD was largest because of high relative humidity that caused hygroscopic growth of particles.
4. Both the PSCF and CWT showed that major input sources were local and short-distance (hundreds of kilometers) transports. But the CWT model revealed considerable long-distance transports of dust from northern China. Southern sources were more obvious in winter that could contribute more anthropogenic aerosols and biomass burning emissions.

These findings gained from long-term LiDAR measurements are significant for improving our understanding of aerosol vertical distributions and decrease uncertainties for studying its effect on radiative forcing in the Yangtze River Delta region of China. The novelty of this study is the employing of LiDAR-derived aerosols-aloft information in backward trajectories models for transport source investigation. Further efforts should be dedicated to combining sun photometer measurements to distinguish aerosol types and verify the results of PSCF and CWT with chemical transport model simulations.

Acknowledgments

This study was supported by the Fundamental Research Funds for the Central Universities (2015XKMS049) and the National Natural Science Foundation of China (41730109). We thank the NOAA Air Resources Laboratory (ARL) for the provision of the HYSPLIT transport and dispersion model and/or READY website (http://www.ready.noaa.gov) used in this publication. Last but not least, special thanks go to the anonymous referees for their constructive and kind comments that help much improve the quality of this work.

References:

Aab, A., Abreu, P., Aglietta, M., et al., 2014. Origin of atmospheric aerosols at the Pierre Auger Observatory using studies of air mass trajectories in South America. Atmos. Res. 149, 120-135.

Ashbaugh, L.L., Malm, W.C., Sadeh, W.Z., 1985. A residence time probability analysis of sulfur concentrations at grand Canyon National Park. Atmos. Environ. 19, 1263-1270.

Atwood, S.A., Reid, J.S., Kreidenweis, S.M., et al., 2013. Analysis of source regions for smoke events in Singapore for the 2009 El Nino burning season. Atmos. Environ. 78, 219-230.

Baars, H., Kanitz, T., Engelmann, R., et al., 2016. An overview of the first decade of PollyNET: an emerging network of automated Raman-polarization lidars for continuous aerosol profiling. Atmos. Chem. Phys. 16, 5111-5137.

Che H, Xia X, Zhu J, et al., 2014. Column aerosol optical properties and aerosol radiative forcing

during a serious haze-fog month over North China Plain in 2013 based on ground-based sunphotometer measurements. Atmos. Chem. Phys. 14(4):2125-2138.

Cheng, I., Xu, X., Zhang, L., 2015. Overview of receptor-based source apportionment studies for speciated atmospheric mercury. Atmos. Chem. Phys. 15,14(2015-07-17) 15, 5493-5536.

Cheng, T., Xu, C., Duan, J., et al., 2015. Seasonal variation and difference of aerosol optical properties in columnar and surface atmospheres over Shanghai. Atmos. Environ. 123, 315-326.

Chew, B.N., Campbell, J.R., Hyer, E.J., et al., 2016. Relationship between Aerosol Optical Depth and Particulate Matter over Singapore: Effects of Aerosol Vertical Distributions. Aerosol & Air Quality Research 16, 2818-2830.

Cho, C., Kim, S.W., Rupakheti, M., et al., 2017. Wintertime aerosol optical and radiative properties in the Kathmandu Valley during the SusKat-ABC field campaign. Atmos. Chem. Phys. 17, 12617-12632.

Cohen, J.B., Ng, D.H.L., Lim, A.W.L., Chua, X.R., 2018. Vertical distribution of aerosols over the Maritime Continent during El Nino. Atmos. Chem. Phys. 18, 7095-7108.

Collis, R.T.H., Russell, P.B., 1976. Lidar measurement of particles and gases by elastic backscattering and differential absorption, Springer Berlin Heidelberg 71-151 pp.

Cottle, P., Strawbridge, K., Mckendry, I., 2014. Long-range transport of Siberian wildfire smoke to British Columbia: Lidar observations and air quality impacts. Atmos. Environ. 90, 71-77.

Draxler, R.R., Hess, G.D., 1998. An overview of the hysplit-4 modeling system for trajectories. Australian Meteorological Magazine 47, 295-308.

Fernald, F.G., 1984. Analysis of atmospheric lidar observations: some comments. Appl Opt 23, 652.

Guo J, He J, Liu H, et al., 2016a. Impact of various emission control schemes on air quality using WRF-Chem during APEC China 2014. Atmos. Environ., 140:311-319.

Guo, J., Liu, H., Wang, F., et al., 2016b. Three-dimensional structure of aerosol in China: A perspective from multi-satellite observations. Atmos. Res. 178-179, 580-589.

Guo, J., Lou, M., Miao, Y., et al., 2017. Trans-Pacific transport of dust aerosols from East Asia: Insights gained from multiple observations and modeling. Environ. Pollut. 230, 1030.

Han, Y., Wu, Y., Wang, T., et al., 2015. Impacts of elevated-aerosol-layer and aerosol type on the correlation of AOD and particulate matter with ground-based and satellite measurements in Nanjing, southeast China. Sci. Total Environ. 532, 195-207.

Han, Y.J., Holsen, T.M., Hopke, P.K., 2007. Estimation of source locations of total gaseous mercury measured in New York State using trajectory-based models. Atmos. Environ. 41, 6033-6047.

He, Q., Li, C., Mao, J., Lau, K.H., Chu, D.A., 2008. Analysis of aerosol vertical distribution and variability in Hong Kong. J. Geophy. Res. 113(D14).

He, Q.S., Li, C.C., Xu, T., et al., 2010. Validation of MODIS derived aerosol optical depth over the Yangtze River Delta in China. Remote Sens. Environ. 114, 1649-1661.

Hennemuth, B., Lammert, A., 2006. Determination of the Atmospheric Boundary Layer Height from Radiosonde and Lidar Backscatter. Bound.-Lay. Meteorol. 120, 181-200.

Hsu, Y.K., Holsen, T.M., Hopke, P.K., 2003. Comparison of hybrid receptor models to locate PCB sources in Chicago. Atmos. Environ. 37, 545-562.

Kang, N., Kumar, K.R., Hu, K., Yu, X., Yin, Y., 2016. Long-term (2002 – 2014) evolution and trend in Collection 5.1 Level-2 aerosol products derived from the MODIS and MISR sensors over the Chinese Yangtze River Delta. Atmos. Res. 181, 29-43.

Klett, J.D., 1981. Stable analytical inversion solution for processing lidar returns. Appl Opt 20,

211-220.

Liu, B., Ma, Y., Gong, W., Jian, Y., Ming, Z., 2018. Two-wavelength Lidar inversion algorithm for determining planetary boundary layer height. J. Quant. Spectrosc. Ra. 206.

Liu, J., Zheng, Y., Li, Z., Connor, F., Maureen, C., 2012. Seasonal variations of aerosol optical properties, vertical distribution and associated radiative effects in the Yangtze Delta region of China. J. Geophy. Res. 117 (D16).

Liu, Q., He, Q., Fang, S., et al., 2016. Vertical distribution of ambient aerosol extinctive properties during haze and haze-free periods based on the Micro-Pulse Lidar observation in Shanghai. Sci. Total Environ. 574, 1502-1511.

Li J, Hu Y, Huang J, et al., 2011. A new method for retrieval of the extinction coefficient of water clouds by using the tail of the CALIOP signal. Atmos. Chem. Phys. 10(11):2903-2916.

Li J, Yi Y, Stamnes K, et al., 2013. A new approach to retrieve cloud base height of marine boundary layer clouds. Geophysical Research Letters, 40(16):4448-4453.

Li J, Huang J, Stamnes K, et al., 2015. A global survey of cloud overlap based on CALIPSO and CloudSat measurements. Atmos. Chem. Phys. 15(1):519-536.

Man, S.W., Qin, K., Lian, H., et al., 2017. Continuous ground-based aerosol Lidar observation during seasonal pollution events at Wuxi, China. Atmos. Environ. 154, 189-199.

Mao, F., Gong, W., Li, J., 2012. Geometrical form factor calculation using Monte Carlo integration for lidar. Optics & Laser Technology 44, 907-912.

Mao, F., Gong, W., Song, S., Zhu, Z., 2013. Determination of the boundary layer top from lidar backscatter profiles using a Haar wavelet method over Wuhan, China. Optics & Laser Technology 49, 343-349.

Qin, W., Liu, Y., Wang, L., et al., 2018a. Characteristic and Driving Factors of Aerosol Optical Depth over Mainland China during 1980–2017. Remote Sens. 10, 1064.

Qin K, Wang L, Xu J, et al., 2018b. Haze Optical Properties from Long-Term Ground-Based Remote Sensing over Beijing and Xuzhou, China. Remote Sensing 10(4):518.

Qin, K., Wu, L., Man, S.W., et al., 2016. Trans-boundary aerosol transport during a winter haze episode in China revealed by ground-based Lidar and CALIPSO satellite. Atmos. Environ. 141, 20-29.

Qu, Y., Han, Y., Wu, Y., Gao, P., Wang, T., 2017. Study of PBLH and Its Correlation with Particulate Matter from One-Year Observation over Nanjing, Southeast China. Remote Sensing 9, 668.

Seibert, P., Kromp-Kolb, H., Baltensperger, U., Jost, D.T., Schwikowski, M., 1994. Trajectory Analysis of High-Alpine Air Pollution Data, Springer US 253-269 pp.

Stohl, A., 1996. Trajectory statistics-A new method to establish source-receptor relationships of air pollutants and its application to the transport of particulate sulfate in Europe. Atmos. Environ. 30, 579-587.

Sun, T., Che, H., Qi, B., et al., 2018. Aerosol optical characteristics and their vertical distributions under enhanced haze pollution events: effect of the regional transport of different aerosol types over eastern China. Atmos. Chem. Phys. 18, 1-45.

Shang H, Chen L, Letu H, et al., 2017. Development of a daytime cloud and haze detection algorithm for Himawari‐imawarient of a daytime clver central and eastern China. J. Geophy. Res. 122(6):3528-3543.

Wang, M., Cao, C., Li, G., Singh, R.P., 2015. Analysis of a severe prolonged regional haze episode in the Yangtze River Delta, China. Atmos. Environ. 102, 112-121.

Wang, Y.Q., Zhang, X.Y., Arimoto, R., 2006a. The contribution from distant dust sources to the atmospheric particulate matter loadings at XiAn, China during spring. Sci. Total Environ. 368, 875-883.

Wang, Y.Q., Zhang, X.Y., Arimoto, R., 2006b. The contribution from distant dust sources to the atmospheric particulate matter loadings at XiAn, China during spring. Sci. Total Environ. 368, 875-883.

Wang, Y.Q., Zhang, X.Y., Draxler, R.R., 2009. TrajStat: GIS-based software that uses various trajectory statistical analysis methods to identify potential sources from long-term air pollution measurement data. Environ. Modell. Softw. 24, 938-939.

Wong, M.S., Nichol, J.E., Lee, K.H., 2013. Estimation of aerosol sources and aerosol transport pathways using AERONET clustering and backward trajectories: a case study of Hong Kong. Int. J. Remote Sens. 34, 938-955.

Wu, Y., Cordero, L., Gross, B., Moshary, F., Ahmed, S., 2012. Smoke plume optical properties and transport observed by a multi-wavelength lidar, sunphotometer and satellite. Atmos. Environ. 63, 32-42.

Wu, Y., Han, Y., Voulgarakis, A., et al., 2017. An agricultural biomass burning episode in eastern China: Transport, optical properties, and impacts on regional air quality. J. Geophy. Res. 122.

Xu, J., Bergin, M.H., Yu, X., et al., 2002. Measurement of aerosol chemical, physical and radiative properties in the Yangtze delta region of China. Atmos. Environ. 36, 161-173.

Yong, H., Wu, Y., Wang, T., et al., 2015. Characterizing a persistent Asian dust transport event: optical properties and impact on air quality through the ground-based and satellite measurements over Nanjing, China. Atmos. Environ. 115, 304-316.

Zachary, M., Yin, L., Zacharia, M., 2018. Application of PSCF and CWT to Identify Potential Sources of Aerosol Optical Depth in ICIPE Mbita. Open Access Library Journal 05, 1-12.

Zeng, Y., Hopke, P.K., 1989. A study of the sources of acid precipitation in Ontario, Canada. Atmos. Environ. 23, 1499-1509.

Zhao, C., Wang, Y. Wang, Q., et al., 2014. A New Cloud and Aerosol Layer Detection Method Based on Micropulse Lidar Measurements, J. Geophy. Res. 119, DOI: 10.1002/2014JD021760.

Zhang, X.Y., Arimoto, R., Zhu, G.H., Chen, T., Zhang, G.Y., 1998. Concentration, size-distribution and deposition of mineral aerosol over Chinese desert regions. Tellus Series B-chemical & Physical Meteorology 50, 317-330.

Zhang, J.L, Liu, P., Zhang, F., Song, Q., 2018. CloudNet: Ground-based Cloud Classification with Deep Convolutional Neural Network, Geophysical Research Letters, doi: 10.1029/2018gl077787

Zheng, C., Zhao, C., 2017. Analysis of Influential Factors for the Relationship between PM2.5 and AOD in Beijing. Atmos. Chem. Phys. 19, 1-57.

Long-term vertical distribution of aerosols during haze and haze-free periods over the YRD region from 3-years(2013-2015) LiDAR observations.

LiDAR observations were combined with backward trajectory model.

PSCF and CWT models were used to investigate aerosol sources.

Pay more attention to the high level aerosols above 1 km.